Citation: Retscher C., G. Kirchengast, A. Gobiet, and A. Hauchecorne, Stratospheric Temperature and Ozone Sounding with ENVISAT/GOMOS Stellar Occultation, in Occultations for Probing Atmosphere and Climate (G. Kirchengast, U. Foelsche, A.K. Steiner, eds.), pp. 299-308, Springer, Berlin-Heidelberg, 2004.

Stratospheric Temperature and Ozone Sounding with ENVISAT/GOMOS Stellar Occultation

C. Retscher[1], G. Kirchengast[1], A. Gobiet[1], and A. Hauchecorne[2]

[1] Institute for Geophysics, Astrophysics, and Meteorology (IGAM), University of Graz, Graz, Austria
christian.retscher@uni-graz.at,
[2] Service d'Aeronomie du CNRS, Verrières-le-Buisson, France

Abstract. The Global Ozone Monitoring by Occultation of Stars (GOMOS) instrument performs high accuracy altitude-resolved global ozone monitoring as well as measurements of other atmospheric trace gases and of temperature. The instrument is mounted on board ENVISAT, the so far largest and most versatile satellite for environmental research. The GOMOS sensor is dedicated to provide measurements from 15 km to 100 km. Due to its high sensitivity, GOMOS is a promising tool to retrieve profiles of atmospheric constituents with high accuracy based on its optical limb transmission data within 250 nm and 940 nm. Ozone is measured, in particular, with spectrometer A covering the spectral range 250 nm to 675 nm. We developed a realistic forward model for simulating GOMOS transmission measurements, which also is a core ingredient for our ozone retrieval algorithm based on the optimal estimation technique. Besides the objective to retrieve ozone profiles using channels within 250 nm to 340 nm, we involve a simultaneous retrieval of NO_2 as well as an exploitation of bending angles from GOMOS star tracking data. GOMOS provides information on bending angles via pointing data of its Steering Front Assembly (SFA) and Stellar Tracking Unit (SATU). From the bending angle we retrieve refractivity profiles (used to improve bended-raypath information within the ozone retrieval process) and, in turn, pressure and temperature profiles (used to improve cross-section modeling, in particular of Rayleigh scattering). The expected precision of the SFA and SATU pointing data enables bending angle errors < 3 μrad (at 10 Hz sampling rate). We show first ozone and temperature retrieval results based on our algorithm, which indicate retrieval errors of < 2 % in ozone throughout the stratosphere/stratopause region and of < 2 K in temperature in the lower stratosphere.

1 Introduction

The observation of high accuracy ozone profiles is crucial for a deeper understanding of changes in the composition of the atmosphere and has a substantial

impact on long-term climate prediction. Stratospheric heating due to the absorption of UV radiation and the importance of ozone as a greenhouse gas are strongly connected to the effects of its continuing depletion. As the primary absorber of solar radiation in the middle UV, ozone plays as well a central role for the biosphere on the Earth surface. Detailed global measurements of the vertical and the horizontal distribution of ozone are therefore necessary to understand physical and photochemical processes. The European Environmental Satellite ENVISAT, launched in March 2002, is ESA's so far most comprehensive venture for probing land, ocean, ice, and the atmosphere. The Global Ozone Monitoring by Occultation of Stars (GOMOS) sensor on-board ENVISAT is a self-calibrating instrument intended to provide data on trace gases such as ozone, NO_2, NO_3, BrO, OClO, as well as O_2 and water vapor. A special instrument design makes it possible to measure reference atmospheric profiles under dark and bright limb conditions obtaining very good global coverage with about 300 high-quality profiles per day and a height resolution of about 1.5 km. GOMOS records the transmission of radiation passing the atmosphere along a path from the star to the instrument. The so-called Spectrometer A measures ozone, NO_2, NO_3, BrO, and OClO within a wavelength range from 250 nm to 675 nm and provides a resolution of 1.2 nm. The Spectrometers B1 and B2 are sensitive within 756-773 nm and 926-952 nm, respectively, with 0.2 nm resolution, and were designed to measure O_2 and water vapor.

Of further importance in this work is the exploitation of GOMOS star tracking and acquisition (SFA/SATU) data for obtaining the bending angle of the rays due to atmospheric refraction. These bending angles allow to derive atmospheric refractivity profiles and subsequently temperature profiles.

Here we present results of our preliminary ozone and temperature retrieval algorithm based on temperature dependent cross-section data of the GOMOS standard cross-section database, standard climatological atmospheric profiles for the trace gases, and CIRA model profiles for background temperature and pressure. data [1, 7].

2 Spaceborne Stellar Occultation with GOMOS

The GOMOS sensor, once fixed on a star, measures transmitted stellar light. During a setting event and due to the motion of the satellite, the line of sight descends through the atmosphere, while the signal gets increasingly attenuated.

The instrument ensures high climate data quality obeying the principle of selfcalibration (normalized intensities), wherefore instrumental long-term drifts can be neglected. GOMOS faces other problems due to the fact that the measured stellar light is occasionally a subject to perturbations from other light sources. Scattered solar light under bright limb conditions, lunar radiation or light coming from auroral emissions into the atmosphere may dominate

the stellar signal, what in turn makes an estimation of such radiation indispensable. Also signal scintillations due to the turbulent atmosphere can be challenging.

The performance of the CCD puts a technical constraint on the selection of the star signal, which has to be a stable flux at visual magnitude brighter than 4 with a star temperature range of favorably 3000 - 30000 K.

2.1 Atmospheric Transmission

The formulation of an appropriate signal propagation geometry is of major importance in order to develop a realistic forward model procedure. We use a realistic yet fast raytracing algorithm, which solves the refractive raypath problem with the star and the satellite position as boundary conditions. The atmospheric transmission is given by Beer-Bouguer-Lambert's law, at each frequency of interest ν, as

$$T_\nu = \frac{I_\nu(s)}{I_\nu(0)} = \exp\left[-\int_{s_1}^{s_2} \sum_i n_i(s')\sigma_{i\nu}(s')ds'\right] . \tag{1}$$

The transmission T_ν is a ratio of the radiation intensity measured in the atmosphere, $I_\nu(s)$, relative to the one, $I_\nu(0)$, measured above (height $\sim$100 km) the atmosphere. The integral is carried out along a refracted ray path s from the star s_1 to the sensor s_2. In our context the number densities n_i and the cross sections $\sigma_{i\nu}$ are associated with the species ozone, NO_2 and NO_3, respectively. In order to reflect the bulk medium, especially important in the lower stratosphere, a factor for the bulk air density with the Rayleigh scattering cross section was introduced as well. In this work a term for the aerosol extinction was neglected, nevertheless, we plan to introduce it in future refinements. Since stars can be assumed to provide a point signal, no further integration over a finite field of view has to be done (as may, e.g., be required for solar occultation).

2.2 Ozone Retrieval

Having a forward model established, we have to find an inverse connection between measurements (transmission data) and targeted state (ozone profile) of the atmosphere. Discrete inverse theory provides such a framework [9], where the forward model can be seen as an algebraic mapping of the state space into the measurement space. We introduce an operator $\mathbf{K}$, which here will be the Jacobian matrix with the dimension $m \times n$ for m measurements and n elements of the state vector. By taking the measurement error ε into consideration the forward modeling reads

$$\mathbf{y} = \mathbf{K}\mathbf{x} + \varepsilon . \tag{2}$$

The sensitivity of measured transmissions $\mathbf{y}$ to the state $\mathbf{x}$, the ozone density profile, can be interpreted as "weighting functions" and seen represented by the rows of $\mathbf{K}$. Because of the generally non-linear Eq. (2), it is obvious that a straightforward solution for $\mathbf{x}$ by direct inversion is not feasible. The direct inverse mapping, if $\mathbf{K}(\mathbf{x}) = \mathbf{K} \cdot \mathbf{x}$ (e.g., linearity applies), would be

$$\mathbf{x}_r = \mathbf{K}^{-g}\mathbf{y} \; , \tag{3}$$

where $\mathbf{K}^{-g}$ denotes a general inverse matrix and $\mathbf{x}_r$ is the retrieved state. As the problem of interest here is ill-posed at high altitudes due to low signal to noise ratio (it may also be over-determined if we use more measurements than unknown states; $m > n$), we cannot directly employ Eq. (3) but rather constrain the solution by incorporating sensible *a priori* information. The Bayesian approach is the method of choice to solve such inverse problems perturbed by noise, where we have rough but reliable prior knowledge of the behavior of a state of interest. We can enhance this prior knowledge in a consistent way by incorporating the measurements with the Bayesian approach.

With the assumption of Gaussian probability distributions and a linearized forward model, we make use of a fast converging iterative optimal estimation algorithm [9],

$$\mathbf{x}_{i+1} = \mathbf{x}_{ap} + \mathbf{S}_i\mathbf{K}_i^T\mathbf{S}_\varepsilon^{-1}\Big[\,(\mathbf{y} - \mathbf{y}_i) + \mathbf{K}_i\,(\mathbf{x}_i - \mathbf{x}_{ap})\,\Big] \tag{4}$$

with the associated retrieval error covariance matrix

$$\mathbf{S}_i = \left(\mathbf{K}_i^T\mathbf{S}_\varepsilon^{-1}\mathbf{K}_i + \mathbf{S}_{ap}^{-1}\right)^{-1} . \tag{5}$$

In Eq. (4), $\mathbf{x}_{i+1}$ is the retrieved, $\mathbf{x}_{ap}$ the *a priori* profile, $\mathbf{y}$ the measurement vector, and $\mathbf{y}_i = \mathbf{K}(\mathbf{x}_i)$ the forward-modeled measurement vector. Key ingredients of Eq. (5) are the *a priori* covariance matrix $\mathbf{S}_{ap}$ and the measurement error covariance matrix $\mathbf{S}_\varepsilon$. The Jacobian (also called weighting) matrix $\mathbf{K}_i$ represents the mapping involved. Index i is the iteration index; the iteration is started by using $\mathbf{x}_0 = \mathbf{x}_{ap}$.

For the elements of $\mathbf{x}_{ap}$ we considered typical errors expected in prior ozone and NO_2 profiles and assumed uncertainties of 20% and 40%, respectively, for the diagonal elements. Off-diagonal elements were modeled by an exponential drop-off correlation of the form

$$S_{ij} = \sigma_i\sigma_j \exp\Big[-\mid z_i - z_j \mid /L\Big] \; . \tag{6}$$

where z_i and z_j denote the height levels between which the covariance is expressed, and where L denotes a correlation length set to 6 km in order to reflect the fact that prior profiles are usually fairly smooth at scales smaller than an atmospheric scale height. Measured ozone profiles may in turn show strong laminar structures with much smaller scales. The standard deviation at a specific height level, σ_i, corresponds to $\sigma_i = (\mathbf{S}_{ap})_{ii}^{1/2}$.

$\mathbf{S}_\varepsilon$ was designed by adopting a 1% standard error at unity transmission and increasing errors with decreasing transmission according to the square-root law (photon detection noise), e.g., $(\mathbf{S}_\varepsilon)_{jj} = 0.01/(y_j^{1/2})$. No interchannel correlation was assumed, thus the off-diagonal elements were set to zero. These error assumptions roughly reflect the measurement error specifications of the GOMOS sensor.

The raytracer-simulated actual transmission measurements $\mathbf{y}$, where superimposed by stochastic error realizations ε (cf. Eq. 2) consistent with the $\mathbf{S}_\varepsilon$ matrix. This was done with the "error pattern method" outlined below for $\mathbf{S}_{ap}$. The forward-modeled measurement vector estimate at any iteration step i, $\mathbf{y}_i = \mathbf{K}(\mathbf{x}_i)$, is used without modification, however.

The *a priori* profiles $\mathbf{x}_{ap}$ where derived by superimposing on the "true" state $\mathbf{x}$ error realizations consistent with the *a priori* error covariance matrix $\mathbf{S}_{ap}$. For this purpose the "error pattern method" was used (e.g., [9, 11]), which exploits the fact that one can decompose $\mathbf{S}_{ap}$ into so-called error patterns obeying $\mathbf{e}_i = \sqrt{\lambda_i}\mathbf{l}_i$. The error patterns $\mathbf{e}_i$ are the eigenvectors of $\mathbf{S}_{ap}$, $\mathbf{l}_i$, weighted by the square-root of the eigenvalues λ_i. In order to construct $\mathbf{x}_{ap}$ statistically consistent with $\mathbf{S}_{ap}$, one adds an error vector $\sum_i a_i\mathbf{e}_i$ to the "true" state $\mathbf{x}$, where the scalar coefficients a_i are normal random deviates drawn from a normalized (zero mean and unit variance) Gaussian distribution.

In general, an error analysis and characterization of atmospheric profile retrievals is an important task for every sensor. Bayesian optimal estimation provides a very suitable framework for this purpose also in case of occultation data [8].

2.3 Temperature Retrieval

In this work, in addition to ozone retrieval, we perform a temperature retrieval based on bending angles profiles, which is well known for radio occultation measurements (e.g. [2, 10, 3]).

Bending angles are extracted from SFA and SATU data gained by the GOMOS sensor. These data products present the movement of the whole CCD within an elevation angle of $61.7° - 69°$ and $11° - 91°$ in the azimuthal direction with a sampling rate of 10 Hz for the SFA. The star image is kept inside the CCD with a sampling of 100 Hz and errors of $\pm$ 10μrad from the central position.

Once we have a total bending angle profile α and accompanying impact parameters a we can apply an inverse Abel transform [2]

$$n(z) = \exp\left[\frac{1}{\pi}\int_{\alpha=\alpha(a_0)}^{\alpha=0} \ln\left(\frac{a(\alpha)}{a_0}\sqrt{\left(\frac{a(\alpha)}{a_0} - 1\right)}\right) d\alpha\right] \tag{7}$$

written here in a favorable from for numerical use by avoiding poles. The $\alpha(a_0)$ and a_0 are the bending angle resp. impact parameter associated with height z, the bottom height of the Abelian integration extending over the height

domain above z. The refractivity follows with $N(z) = (n(z) - 1) \times 10^6$, which can be converted into pressure p by integrating the hydrostatic equation. A temperature profile can be subsequently derived from p and N by the equation of state (ideal gas law).

At heights above 30 km, where the bending angles become small due to the increasingly tenuous atmosphere, the decreased signal-to-noise ratio calls for suitable high-altitude initialization of the bending angle profiles in order to feed the Abel transform Eq. (7) with adequate data.

The statistical optimization [10] optimally combines measured and background (*a priori*) bending angle profiles leading to the most probable bending angle profile [3]. An optimal solution is feasible via

$$\alpha_{opt} = \alpha_b + \left(\mathbf{B}^{-1} + \mathbf{O}^{-1}\right)^{-1} \mathbf{O}^{-1}(\alpha_o - \alpha_b) \;, \tag{8}$$

where α_b is the background and α_o the observed bending angle profile, respectively. The matrices $\mathbf{B}$ and $\mathbf{O}$ express the background and the observation error covariances, respectively. Similar to Eq. (6) we define

$$B_{ij} = \sigma_i \sigma_j \exp\left[|a_i - a_j| / L\right] \;, \tag{9}$$

with impact parameters a at different height levels i and j. The correlation length L was set to 6 km for $\mathbf{B}$, while we find $L = 1$ km appropriate for $\mathbf{O}$, which used the same form as Eq. (9). As a background profile we chose a CIRA climatology. Background errors (such as σ_i and σ_j) were assumed to be 20% in line with radio occultation literature(e.g. [3, 4]). The observation errors were estimated from the root-mean-square deviation of the observed data from the background at high altitudes (70 - 80 km), where noise dominates the measured signal. Details on the statistical optimization scheme used are found in [4], which also provides further information on the full retrieval chain from bending angle to temperature.

3 Preliminary Retrieval Results

We performed tests of our preliminary algorithm based on a quasi-realistic occultation event. The geometry of the event, displayed in Figure 1, was provided by an enhanced EGOPS (End-to-end Generic Occultation Performance Simulator) [5, 6], a comprehensive occultation.

In this baseline study we adopted spherically symmetric atmospheric profiles in the forward modeling, though the fast ray tracing algorithm calculates the raypath by taking also horizontal variations of refractivity into account (this capability will be useful in future more elaborated application). We simulated the scanning of the atmosphere and retrieved ozone profiles with a sampling rate of 2 Hz, consistent with GOMOS sampling, from altitudes of 90 km to 15 km. Simulated transmission profiles, after carrying through the forward modeling according to Eq. (1), are displayed in Figure 2. In contrast

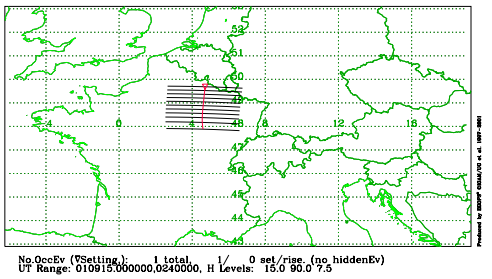

Fig. 1. Test occultation event shown with 7.5 km spacing between rays from 90 km to 15 km along the tangent point trajectory in nadir view over north-eastern France and southern Belgium. The bundle of parallel lines illustrates the raypaths for ±150 km about the tangent point, roughly reflecting the horizontal resolution of the occultation data.

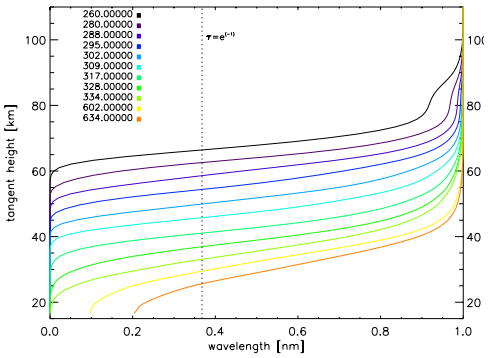

Fig. 2. Simulated transmission profiles based on including O_3, NO_2, and NO_3 absorption as well as Rayleigh scattering for the 11 channels used in this baseline study.

to the GOMOS operational retrieval, where the forward model uses all many hundred channels of Spectrometer A, we restrict ourselves to only eleven well selected ozone channels (here 260, 280, 288, 295, 302, 309, 317, 328, 334, 602, 634 nm) as Figure 2 illustrates. We therefore gain vastly in computational efficiency while retaining quality of the ozone profiles on which we focus. The current operational algorithm simultaneously retrieves all accessible species (see section 2). The channel selection will be further optimized in the future, especially within 320 and 340 nm.

In the selected wavelength ranges ozone absorption is most pronounced, while ozone cross sections show only slight temperature dependencies (nevertheless such temperature dependencies are accounted for). The ranges provide the most favorable GOMOS channels for ozone retrieval. In order to ensure

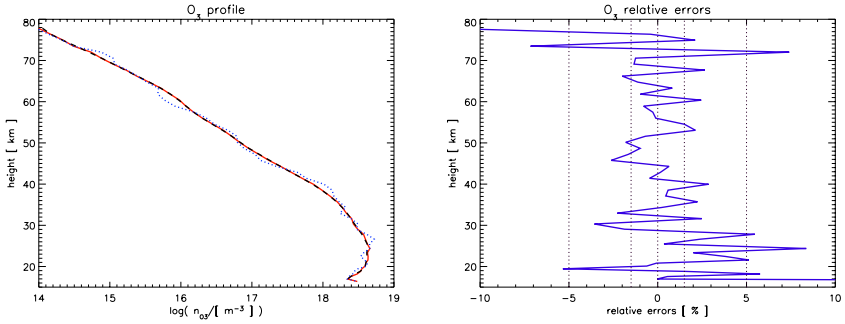

Fig. 3. (a) Example of retrieved ozone number density profile (solid line) and an *a priori* profile (dotted line) with the "true" profile (dashed line) shown for reference. (b)Relative errors of the retrieved ozone density profile shown in Figure 3 (difference retrieved minus "true").

high reliability of retrieved ozone profiles also at heights where the spectral region > 320 nm is relevant, we included NO_2 into the state vector retrieved NO_2 simultaneously as a by-product. Using the transmissions shown in Figure 2, perturbed by noise as discussed in section 2 above, the retrieval was carried out according to Eqs. (4) and (5). The algorithm consumed up to three to four iterations after which convergence was robustly achieved. Figures 3 and 4 illustrate the retrieval results obtained for a representative test case. RMS errors of $< 2\%$ in ozone density are seen between 30 and 70 km, which is encouraging for further advancements of the algorithm. The larger errors seen below about 30 km may have their origin in the temperature dependencies of the standard GOMOS ozone cross sections and in the channel selection. Further enhancements will be made to mitigate these errors. Also the high-altitude (> 70 km) treatment will be improved.

Stratospheric temperature could be determined with high accuracy from the SFA/SATU bending angle data. In our test we superimposed errors of $\pm 3\mu$rad (corresponding to a sampling rate of 10 Hz) on the true profiles denoted as black solid lines in the Figure 4. Retrievals, where no optimizations was used (dashed lines) show a clear deviation from 20 km up to higher altitudes. Errors < 3 K could only be found below 30 km. This demonstrates how initialization errors at high altitudes propagate downward influencing temperature errors even at heights around 20 km. Statistical optimization in turn leads to a significantly improved bending angle profile ensuring temperature errors of < 1 K below 25 km and < 2 K below 35 km.

4 Summary and Conclusions

We developed an optimal estimation algorithm for retrieval of atmospheric profiles from ENVISAT/GOMOS-measured transmission data. In this study

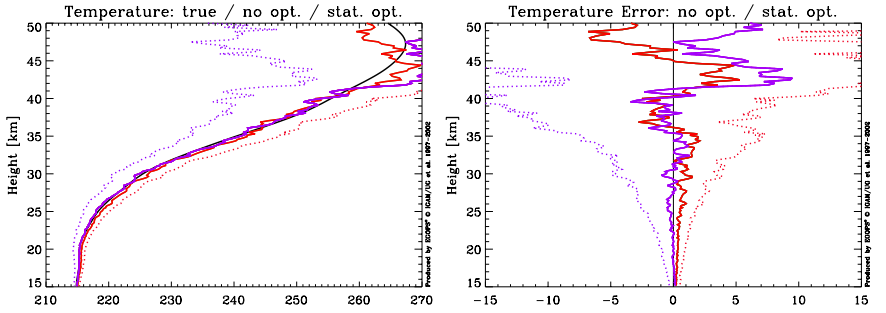

Fig. 4. (a) Two realizations of temperature profiles with (solid grey lines) and without (dashed grey lines) statistical optimization applied; the smooth profile (solid black line) is the "true" profile (b) Corresponding errors (difference retrieved minus "true") of the two error realizations of temperature profiles with and without statistical optimization applied.

ozone profiles were retrieved, which is the primary focus of the algorithm, though the whole processing chain is capable of retrieving other trace gases simultaneously.

Furthermore, we applied refractive occultation retrieval to bending angle data from GOMOS star tracker data (SFA/SATU) gaining refractivity and temperature profiles. A simultaneous exploitation of atmospheric transmission and bending angles was not yet performed in this study but will be introduced as a future enhancement. This enhancement will allow to simultaneously retrieve ozone and temperature profiles in the stratosphere as well as atmospheric refractivity and density, which can be used to improve the background fields required by the raytracing. These improvements will further boost the ozone retrieval.

In conclusion, the approach adopted for an efficient retrieval of ozone profiles has yielded encouraging preliminary results so far, with ozone profile accuracy $< 2\%$ from mid stratospheric up to high mesospheric regions. Temperature errors based optimally initialized bending angle profiles show a high retrieval quality with errors of < 2 K below 35 km and < 1 K below 25 km. We are thus confident to be able to start applying the algorithm to real GOMOS data by mid 2003.

Acknowledgements. The authors gratefully acknowledge discussions with and support by U. Foelsche, M. Schwärz, C. Rehrl, and J. Ramsauer (IGAM, Univ. of Graz, Austria). The European Space Agency is thanked for operating the ENVISAT satellite and for its related Announcement of Opportunity for free access to ENVISAT data, which will be vital in subsequent work. C.R. received financial support for the work from ENVISAT Project AO-620/Part-I funded by the Austrian Ministry for Traffic, Innovation, and Technology and carried out under contract with the Austrian Space Agency.

References

[1] Acri SA et al. (1998) Gomos high level algorithms definition document. Technical report, ACRI S. A., France, Finnish Meteorol Institute, Service d'Aronomie du CNRS, and Institut d'Aronomie Spatiale de Bruxelles, http://envisat.esa.int/support-docs/.

[2] Fjeldbo GF, Eshleman VR, Kliore AJ (1971) The neutral atmosphere of venus as studied with the mariner v radio occultation experiments. Astron J 76: 123–140

[3] Healy SB (2001) Smoothing radio occultation bending angles above 40km. Annales Geophysicae 19: 459

[4] Gobiet A, Kirchengast G (2002) Sensitivity of atmospheric profiles retrieved from gnss occultation data to ionospheric residual and high-altitude initialization errors. Technical report, ESA/ESTEC No. 1/2002: IGAM, University of Graz, Austria, 58 pp.

[5] Kirchengast G (1998) End-to-end gnss occultation performance simulator overview and exemplary applications. Wiss. Ber. 2/1998: IGAM, University of Graz, Austria, 138 pp.

[6] Kirchengast G, Fritzer J, Ramsauer J (2002) End-to-end gnss occultation performance simulator version 4 (egops4) software user manual (overview and reference manual). Technical report, ESA/ESTEC-3/2002: IGAM, University of Graz, Austria, 472 pp.

[7] Paulsen T (2000) Gomos level 1b/2 algorithm description document for enviview pre-release. Technical report, ESA Doc. PO-TN-ESA-GM-1019, ESA/ESTEC, Noordwijk, Netherlands

[8] Rieder MJ and Kirchengast G (2001) Error analysis and characterization of atmospheric profiles retrieved from gnss occultation data. J Geophys Res 31755–31770

[9] Rodgers CD (2000) Inverse Methods for Atmospheric Remote Sounding: Theory and Pratice. World Sci Publ, Singapore

[10] Sokolovsky S, Hunt D (1996) Statistical optimization approach for gps/met data inversions. In: URSI GPS/Met Workshop, Tuscon, Arizona

[11] Weisz E (2001) Temperature profiling by the infrared atmospheric sounding interferometer (iasi): Advanced retrieval algorithm and performance analysis. Wiss Ber 2/1998: IGAM, University of Graz, Austria